JLAB12 Activity report 2020

V. Lucherini, M. Mirazita (Resp.), D. Orecchini(Tecn.), A. Orlandi(Tecn.),
O. Soto (INFN fellowship), S. Tomassini

1 Introduction

The JLAB12 group of LNF participates in the physics program carried on by the CLAS collaboration in the Hall B of the Jefferson Laboratory (JLab). The LNF group has been deeply involved in the analyses of the physics data, in particular in the work that lead to the first physics publications with CLAS12. In parallel, the construction of the second RICH module is progressing.

2 The CLAS12 RICH

The detector is composed by an aerogel radiator, an array of multianode photomultiplier tubes (MAPMTs) for the Cherenkov light detection and a mirror system. All these elements are contained in a large trapezoidal box, of approximate height of 3.5 m and large base of about 4 m.

The radiator is composed by tiles with squared shape 20×20 cm^2 as well as smaller pentagonal, trapezoidal or triangular tiles to accomodate with the detector shape. The total number of tiles is 102, assembled in two sections: the forward angle one made by one layer with 2 cm thickness and the large angle one made by two layers with 3 cm thickness each.

The mirror system is composed by 10 carbon fiber spherical mirrors and 7 glass planar mirros, for a total surface of about 10 m^2. The goal of the mirror system is to contain as much of the produced Cherenkov inside the detector and to direct them toward the photodetector array.

The photodector array uses 391 MAPMT Hamamatsu H8500 and H12700. These two types of tubes are composed by a matrix of 8×8 matrix of pixel with about 6 mm pixel size, with a total of 25024 independent readout channels.

The readout electronics is based on the MAROC3 chip, a 64 channel microcircuit dedicated to MAPMT pulse processing. Each channel offers a low impedence adjustable gain preamplifier followed by a highly configurable shaping section, and produces both prompt logic pulses from an adjustable threshold discriminator. The MAROC is configured and read out by a FPGA optically linked with the data acquisition node. The front-end electronics is organized in compact units mechanically designed to fit the MAPMT dimensions and serving two or three MAPMTs each, thus allowing the tessellation of large surfaces with minimum dead space and material budget.

2.1 Study of the performance of the first RICH module

During the year 2020, the first large scale production of CLAS12 data has been provided to the users for the first physics publications. These data allowed a detailed study of the RICH performance and preliminary results have been reported to the CLAS Collaboration. At the present stage of the analysis, only Cherenkov photons detected on the photomultiplier plane without reflections on the mirrors have been included, because the precise alignment of the internal elements of the detector has not been completed yet. For this reason, the kinematic coverage of the results is limited in both

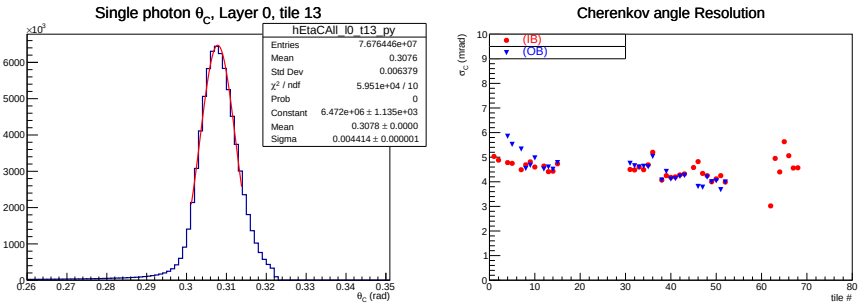

Figure 1: *Left plot: typical distribution of the singler photon Cherenkov angle for electrons hitting one of the 2 cm thickness aerogel tiles. Right plot: comparison of single photon resolution for the two polarities of the CLAS12 torus field.*

polar angles (large angle particles have large fraction of photons hitting the spherical mirrors) and azimutal angles (particles close to the lateral edges of the RICH have large fraction of the photons hitting the lateral mirrors). In addition, we may also expect some contribution of reflected photons in the central part of the RICH, due to the bending of the charged particles in the solenoidal and toroidal fields of CLAS12.

2.1.1 Characterization of the RICH with electrons

The identification of the electrons is not in the goals of the RICH. However, they provide a very powerful tool for the characterization the RICH response and to determine all the relevant parameters for the hadron identification. Electrons are selected using the CLAS12 general particle identification algorithm, that combines information from the Drift Chambers, the time-of-flight scintillators and the electromagnetic calorimeters. Distributions of the single photon Cherenkov angle are produced for each aerogel tiles and fitted with a gaussian curve to extract mean and σ. Being particle with $\beta = 1$, their Cherenkov emission angle does not depend on the momentum, so these distributions allow the extraction from the experimental data of the refractive index through the relation

$$n = \frac{1}{\cos\theta_C} \tag{1}$$

An example of one of these distributions is shown in the left plot of the Fig. 1. We can extract from the fit a single photon resolution $\sigma = 4.4$ mrad. In the right plot of the Fig. 1 we show the single photon resolution as a function of the tile number, comparing results obatained from data with two opposite polarity of the CLAS12 torus field. The two data provide very similar results for most of the tiles. Some discrepancy is found only for the first tiles, in the very forward angles, where the CLAS12 tracking system still requires some fine tuning. Although we expect some improvement once the alignment process will be completed, the measured resolutions are already below or very close the 4.5 mrad design specification in the forward direction.

2.1.2 Hadron identification in the RICH

The hadron identification in the RICH reconstruction algorithm is based on a likelihood approach, taking into account all the possible combinations of hadron mass candidates for all the charged tracks in the detector. However, being the alignment of the internal elements of the detector not completed yet, a simpler approach has been used here. First of all, only events with one charged track in the RICH have been selected. Then, for each particle hypothesis, a Cherenkov

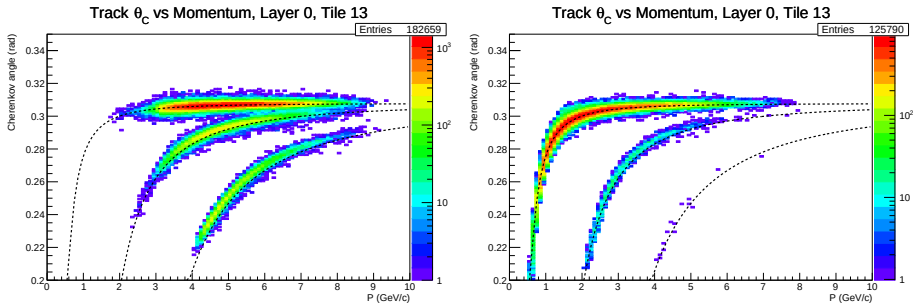

Figure 2: *Average Cherenkov angle as a function of the momentum for positive (left) and negative (right) hadrons identified in the RICH for one typical aerogel tile.*

angle fiducial interval is defined and the the number of photons within this region is counted. This fiducial region is defined as $[\theta_h - 3\sigma_h, \theta_h + 3\sigma_h]$, where θ_h and σ_h are computed based on the previous electron results and knowing the momentum from the tracking system. The particle hypothesys that maximizes the number of photons is assumed as true and the average Cherenkov angle of the track is computed. An example of the resulting Cherenkov angle as a function of the momentum is shown in Fig. 2 for positive and negative hadrons. We clearly see the bands corresponding to the various hadron species, with the pions and kaons well separated up to momenta of about 6 GeV/c, while the proton band is well separated form the kaon over the whole momentum range. We expect an improvement in the kaon/pion separation at the highest momenta once the alignments will be completed and the reflected photons will be included.

2.1.3 Physics analysis with the RICH

To have a first look at the kaon identification with the RICH, we can select semi-inclusive eKX events, where the kaon is going in the RICH while the electron is identified in one of the CLAS12 sector not instrumented with the RICH. In order to maximize the statistics, we also apply the following loose Deep Inelastic Scattering cuts

- $Q^2 > 2$ GeV^2/c
- $W > 1$ GeV
- $y < 0.9$

In Fig. 3, we show distributions of the missing mass for positive (left) and negative (right) kaons. The black full lines in the plots represent the case when all the kaons identified by the CLAS12 time-of-flight are used, while the dashed black lines represent events within the RICH fiducial region. The blue lines represent the case when the kaons identified in the RICH are selected.

We see that the histograms using the CLAS12 identification show unphysical structures, in particular close to the nucleon mass in the eK^+X distribution and close to the Δ^{++} mass in the eK^-X distribution. These fake structures mostly disappear when the RICH identification of kaons is used. In addition, a large signal-to-background improvement in all the Λ peaks are obtained with the RICH. These plots demonstrate that, although the ultimate performance has not been reached yet, the RICH is already able to provide reliable kaon identification in most of the momentum range.

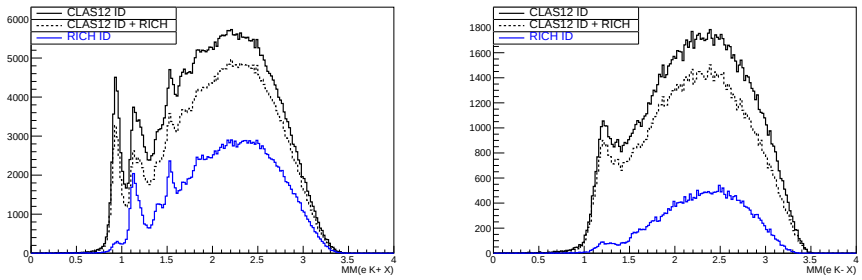

Figure 3: *Average Cherenkov angle as a function of the momentum for positive (left) and negative (right) hadrons identified in the RICH for one typical aerogel tile.*

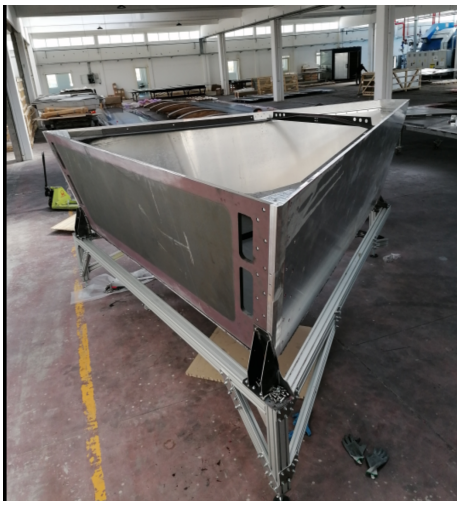

Figure 4: *Assembly test of the second RICH module.*

2.2 Construction of the second RICH module

The contruction of the second RICH module, with the same geometry of the first one, is currently underway under the supervision of the physicists, technologits and technicians of the LNF group. The status of the construction is still on time for having it installed inside CLAS12 by the end of the year 2021, but the present pandemic crisis could delay the installation to the 2022.

2.2.1 Mechanical structure

The construction of the mechanical structure has been completed and an assembly test has been performed by the end of the year 2019 (see Fig. 4). After completion of the test, the module has been dismounted and send for the final cleaning and painting of all the components. The shipment to JLab is currently in preparation.

2.2.2 Mirrors

All the planar mirrors have been produced and tested, with the only exeption of the frontal mirror B2, which will be completed in 2021. In Fig. 5 we show a picture of the frontal mirror B1 and the

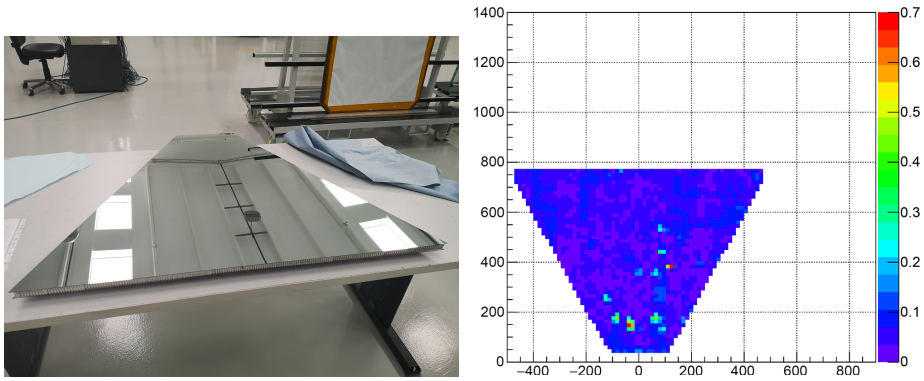

Figure 5: *Picture of the frontal mirror B1 and results of the slope profile measurements.*

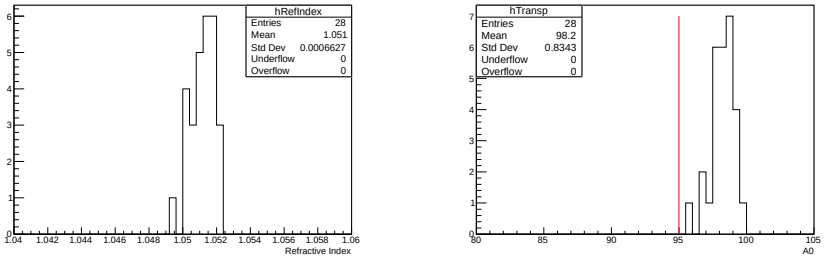

Figure 6: *Results of the characterization measurements of the squared tiles of the 2 cm thickness sector: refractive index at the reference wavelength of 2 cm (left) and transparency coeeficient (right), with the vertical line indicating the minimum requirement of 0.95.*

results of the measurement of the profile of the surface. We see that the local slope of the surface of the mirror exceeds the design limit of 0.3 mrad only in few spots. We found on average on all the mirrors produced so far that only about 1% of the surface slope exceeds the limit, with an improvement of more than a factor of 2 with respect to the mirrors of the first RICH module.

The production of the spherical mirrors has been started by placing the order by the end of 2020. A revision of the design of the carbon fiber structure supporting these mirrors in underway, with the goal of reducing the costs and improving the stiffness. We plan to place the order for the support by the first months of 2021.

2.2.3 Aerogel

The production of the aerogel tiles has been almost completed in 2020. All the large squared tiles have been produced, while the last smaller lateral tiles with triangular, trapezoidal and pentagonal shape of the 3+3 cm thickness sector is being completed. We plan to have a final shipment to JLab by the spring 2021. The optical quality of the tiles showed a slight improvement with respect to the ones of the first module. As an example, we show in Fig. 6 the refractive index measured at the reference wavelength of 400 nm (on the left) and the transparency (on the right) measured for all the squared tiles of the 2 cm thickness sector.

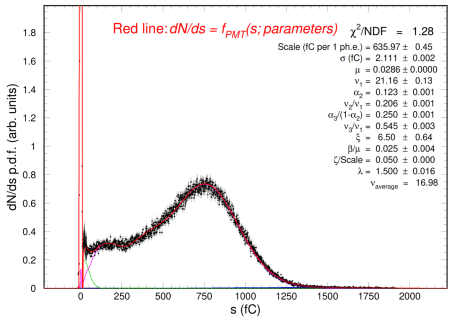

Figure 7: *Typical single photo-electron spectrum measured for one pixel of a MAPMT.*

2.2.4 Photomultipliers

The production of the multi-anode photomultipliers is shared with the JLab. About 80% of the 400 MAPMTs have been produced and delivered to JLab. The characterization tests with a laser test stand using the same readout electronics used in the RICH are underway. So far, only 4 MAPMTs have been found out of specifications and sent back to the Hamamatsu for replacement. In Fig. 7 we show a typical spectrum measured illuminating one pixel of one MAPMT with a laser beam at singl photon level. We remind to the summary paper [1)] on the tests of the MAPMT of the first module for the explanation of the fit of the measured spectrum.

3 Physics analysis

The LNF groups is involved in data analysis aiming at the study of the internal structure of the nucleon through the measurements of Semi-Inclusive Deep Inelastic Scattering (SIDIS) of polarized electrons on a fixed target and looking at final states with one or more hadron. The underlying reaction mechanism can be schematized with a virtual photon exchanged by the incoming electron and the target that interacts with one of the quark composing the nucleon. After the interaction, the struck quark fragments into the observed hadron(s). The presence of the final hadrons allows the access to a number of spin-orbit correlations between the transverse momentum and the spin of the quarks with the transverse momentum of the hadron. The relevant quantities in these measurements are the Transverse Momentum Dependent (TMD) functions, 3-dimensional extensions of the well known collinear Partonic Distribution Functions (PDFs).

3.1 Analysis of CLAS12 data

During the year 2020, the LNF was highly involved in the work that lead the CLAS Collaboration to the first two physics publications with the new CLAS12 data. These two publications reported the measurements of the single Beam Spin Asymmetry (BSA) in SIDIS reactions with one [2)] and two [3)] charged pions in the final state. Physicists of the LNF participated to the work carried out to calibrate the CLAS12 detector, to study its performance, select the fiducial regions of the various sub-detectors where the response is flat and well under control, define the correction functions necessary to reach the ultimate performance and to cross-check all the steps of the analysis. They were also part of the various review committee that examined the analysis work and approved it for the publication.

3.2 Multiplicity measurements in the SIDIS two-pion final state with CLAS12 data

Orlando Soto of the LNF group is responsible for the analysis aiming at the the measurement of the multiplicity in the SIDIS two charged pion final state with CLAS12 data taken with both hydrogen and deuteron targets. The multiplicity is defined as the ratio of the SIDIS cross section to the inclusive one:

$$M(x_B, Q^2, z, M_{\pi\pi}, P_T) = \frac{d\sigma^{\pi\pi}}{d\sigma^{incl}} \tag{2}$$

where x_B and Q^2 are the usual DIS variable, z is the fraction of the incoming virtual photon energy carried by the pion pair, $M_{\pi\pi}$ and p_T are the invariant mass and transverse momentum of the pair. Decomposing the cross sections in terms of PDFs, one obtains the following expression, up to kinematical factors:

$$M(x_B, Q^2, z, M_{\pi\pi}, P_T) \approx \frac{\sum_q e_q^2 f_1^q D_1^q}{\sum_q e_q^2 f_1^q} \tag{3}$$

where the sum runs over the quark flavor q with charge e_q, f_1^q is the well know unpolarized PDF and D_1^q is the, basically unknown, dihadron fragmentation function (FF). Combining data on hydrogen and deuteron target, and using isospin relations between the PDFs on proton and neutron, one can extract from the data the FF for the two quarks *up* and *down* separately.

Experimentally, the multiplicity can be written as ratio of acceptance-corrected number of dihadron and inclusive events. As such, a crucial step of the analysis is the estimate of the acceptance correction. Therefore, a large part of the work performed during the 2020 as been devoted to the careful verification and validation of the CLAS12 Monte Carlo simulations against the experimental data. The massive production of Monte Carlo data is now underway on both proton and deuteron targets.

Preliminary results of the multiplicity analysis have been presented at the 2020 SIF Congress [4]. In Fig. 8, we show an example of the results from the proton target data. Here, one particular bin in Q^2 and P_T has been chosen. Each small plot represent one bin in x_B (along the vertical scale) and z (along the horizontal scale) and shows the $M_{\pi\pi}$ dependence of M.

3.3 Two pion measurements with CLAS data

The measurement of the BSA in the SIDIS electroproduction of charged pion pairs with old CLAS data has been completed under the responsibility of the LNF group in 2020 and published [5]. The BSA is defined (up to some kinematic factor) as the ratio:

$$BSA \propto \frac{d\sigma_{LU}}{d\sigma_{UU}} \tag{4}$$

where $d\sigma_{UU}$ is the SIDIS unpolarized cross section and $d\sigma_{LU}$ is the cross section term proportional to the helicity of the incoming electron. Experimentally, the BSA can be written as

$$BSA = \frac{1}{P_B} \frac{N^+ - N^-}{N^+ + N^-} \tag{5}$$

where $N^\pm$ are the number events with positive or negative electron helicity and P_B is the average beam polarization.

From the theoretical point of view, the BSA is proportional to the only azimuthal harmonic $\sin\phi_R$, where ϕ_R is the azimuthal angle of the relative momentum of the pion pair:

$$BSA \propto A_{LU}^{\sin\phi} \sin\phi \tag{6}$$

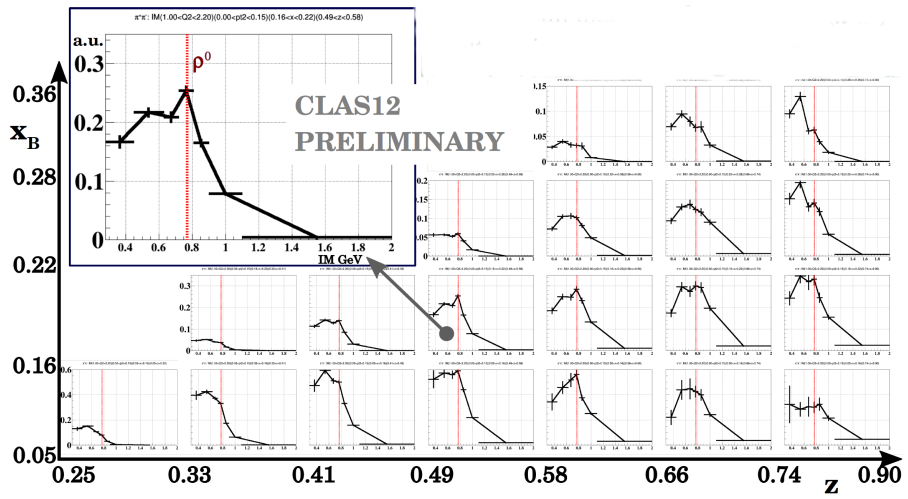

Figure 8: *Two charged pion multiplicity as a function of $M_{\pi\pi}$ in bins of x_B and z and in the bin $1.0 < Q^2 < 2.2$ GeV^2 and $0< P_T < 0.15$ GeV/c. Data on proton target.*

where the $\sin\phi_R$ moment of the BSA $A_{LU}^{\sin\phi}$ can be written as a combination of quark PDFs and FFs. All other modulations of the SIDIS cross section should disappear after integration over the relevant angles.

However, this could not be true in presence of an highly asymmetric acceptance, as it is the case of the CLAS detector. The careful analysis of the experimental data demonstrated that a reliable extraction of A_{LU} can be performed only by fitting the BSA in a 2D binning over the two angles ϕ_R and ϕ_H, where ϕ_H is the azimutal angle of the total momentum of the hadron pair, using the function

$$BSA = c_1 \sin\phi_R + c_2 \sin(\phi_H - \phi_R) \tag{7}$$

The extracted $\sin\phi_R$ moment of the BSA as a function of the relevant kinematic variables is shown in Fig. 9. Although with limited statistical precision, these data represent a pioneering study that for the first time accounted for different systematic effects that are crucial in higher statistics experiments, as for example the one performed with CLAS12 data [3].

Under some theoretical assumptions, the measured BSA is proportional to the chiral-odd higher-twist PDF $e(x)$, that is related to the nucleon scalar charge and to the nucleon sigma term. Work is in progress in collaboration with theorists to attempt a first extraction of $e(x)$ from out dihadron BSA data.

References

1. P. Degtiarenko, Nucl. Instrum. Methodes A 872 (2017) 1

2. S. Diehl *et al.* (CLAS Collaboration), "First Multidimensional, High Precision Measurements of Semi-Inclusive π^+ Beam Single Spin Asymmetries from the Proton Over a Wide Range of Kinematics", arXiv:2101.03544, submitted to Phys. Rev. Lett., (2021).

3. T.B. Hayward *et al.* (CLAS Collaboration), "Observation of Beam Spin Asymmetries in the Process $ep \to e\pi^+\pi^- X$ with CLAS12", arXiv:2101.04842, submitted to Phys. Rev. Lett., (2021)

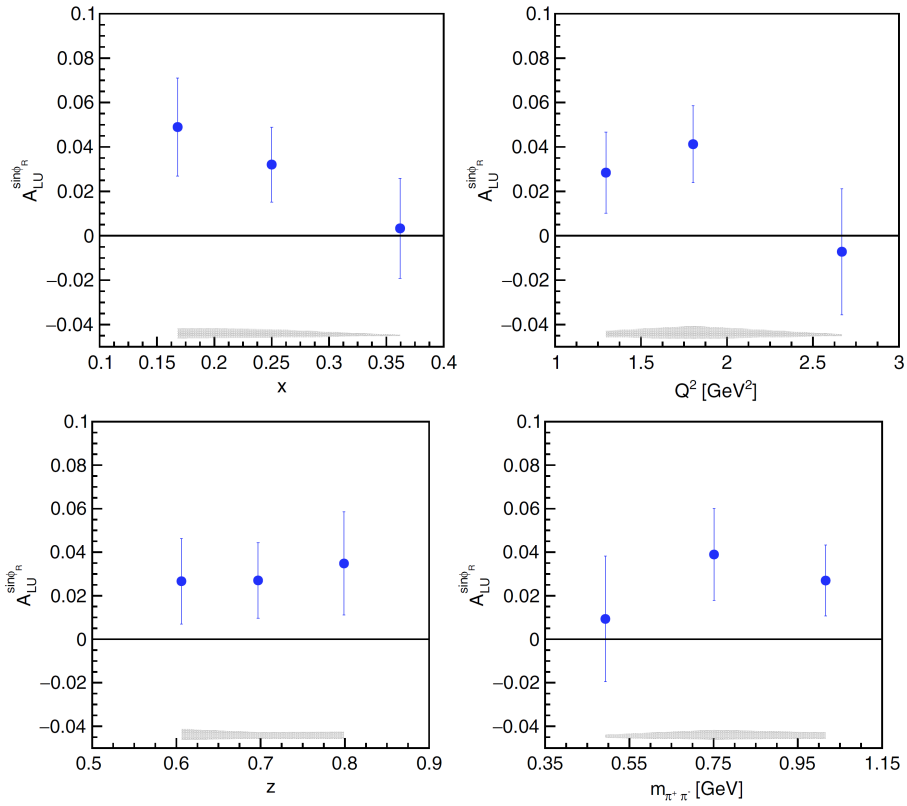

Figure 9: *The* $\sin\phi_R$ *moment of the BSA as a function of* x_B *(top left)* Q^2 *(top right),* z *(bottom left) and* $M_{\pi\pi}$ *(bottom right) extracted from the CLAS data. The error bars represent the statistical uncertainty, grey band on the bottom represent the systematic uncertainty.*

4. https://www.sif.it/attivita/congresso/106

5. M. Mirazita *et al.* (CLAS Collaboration), "Beam-Spin Asymmetry in Semi-Inclusive Electroproduction of Hadron Pairs", Phys. Rev. Lett 126, 062002 (2021).